Analysis of air flow in feeders for gas burners

João Nuno Carlota Duarte

Instituto Superior Técnico - Universidade Técnica de Lisboa
Departamento de Engenharia Mecânica, Lisboa, Portugal
jncduarte@gmail.com

17th October 2011

Abstract

With the need of attaining lower NO_X emissions from water heater burner units, the industry is studying a new generation of domestic water heaters, in which primary air is not naturally entrained, but fed by a ventilator instead.

The aim of this work is analysing the flow rate distribution at the diffuser outlet which drives the air to the burning system, being required that the flow rate distribution is homogeneous for the nine channels. For such, it is necessary to know the flow at the ventilator outlet and to test the diffuser configuration. The experimental characterization is made using Particle Image Velocimetry and microphone measurements, as to find recirculation zones in the diffuser. Measurements are carried out for three ventilator rotational speeds. After processing the data, velocity profiles are integrated over the area to compute the flow rate supplied by this assembly. One concludes that the original diffuser configuration does not guarantee a homogeneous flow rate distribution. The static pressure and fluctuation tests indicate that there is a recirculation zone inside the diffuser. Taking these results, a new diffuser channel geometry is conceived. Since flow behavior is understood and a new diffuser geometry is proposed, all the objectives of the present work are achieved.

I -- Introduction

Burners used in traditional water heaters need an injector that supplies the fuel and work in partial premixed conditions (Jones, 1989). They work on the ejector pump principle, where a high velocity fuel jet reaches the contraction zone of the burner. There, the velocity increases and consequently the pressure decreases, leading to air entrainment due to momentum transfer from the high velocity fuel jet to the surrounding air. Previous master thesis done at Instituto Superior Técnico approached the effect of burner geometries and pilot flame systems in pollutant emissions of Bosch water heaters (Duarte, 2008; Rato, 2009), finding that they burn under slightly rich regimes with high NO_X and low CO_2.

Nowadays, the energy crisis and fuel prices are leading to tighter pollutant emission limits. Thus, it is necessary to improve combustion processes. In particular, there is a specific need of domestic water heater manufacturers to lower NO_X emissions from their models by burning on lean flame regimes.
A recent alternative type of domestic water heaters must be taken into account. In those, primary air is not naturally drawn into the burners -- instead, it is forced by a ventilator through an ensemble which comprehends a diffuser and the burner matrix, allowing to go to lean burning regimes. This configuration is used in the pressurized burner project as an attempt to work on lean pre-mixed flames. The motivation for the present thesis comes from industry's necessity to understand how does the forced air flow affect flame behavior and NO_X emissions. Still, as the pressurized burner project involves a new geometry burner assembly, that makes arise some problem concerning fluid mechanics.

Thereafter, the main idea of this work is to study the flow across the ventilator and try to obtain a homogeneous flow distribution at the diffuser exit -- that is begin by testing a manufacturer's original configuration and, if necessary, propose modifications that can lead to better results. To reach this purpose, the velocity field at both the ventilator outlet and diffuser exit is characterized by Particle Image Velocimetry (PIV) and pressure measurements.

It is important to refer that the water heater manufacturer ordered a numerical simulation for both the ventilator and diffuser.

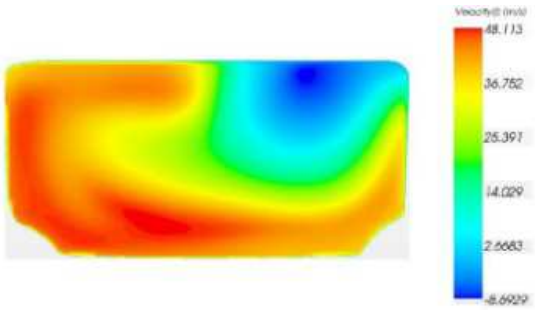

Figure 1 - Vertical component of velocity at the ventilator exit (From a private report).

II -- Experimental Setup

The water heater studied in this work is composed by three zones: i) a radial ventilator which forces air into the burner; ii) a diffuser which distributes the flow to the burners and iii) burner slots, where the primary air and the injected gas form a mixture.

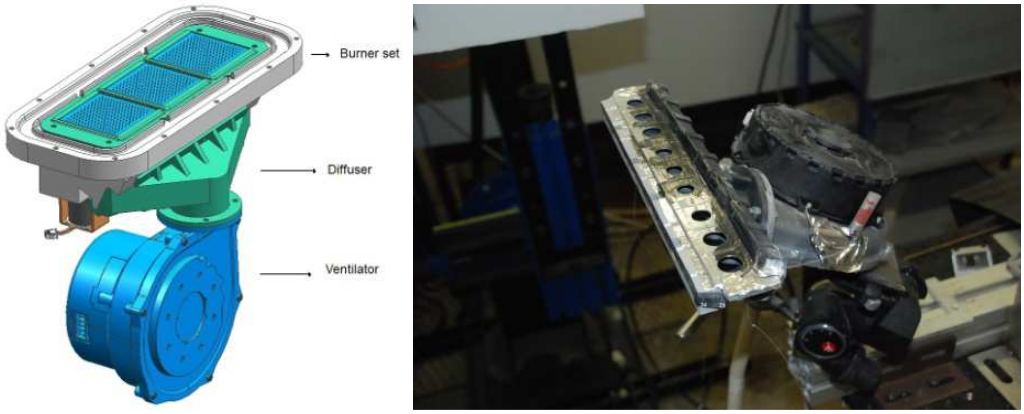

Figure 2 – Bosch's pressurized burner system drawing (left) and ventilator and diffuser assembly (right).

The diffuser is responsible for feeding the burner set with primary air and it is required that the air distribution at the diffuser exit is as homogeneous as it gets, as to have approximately the same amount of air entering each burner slot. This configuration includes a plate with holes at the diffuser outlet, as to *force* air flow rate to be homogeneous across each hole.

PIV is a non-intrusive method for measuring velocity fields in fluid flows and consists in seeding a flow with tracer particles, which are illuminated by a laser beam. The light reflected by the particles is captured into image frames and software allows computing particle displacement in a certain time interval. Consequently, one gets the velocity of each particle dragged by the flow in analysis.

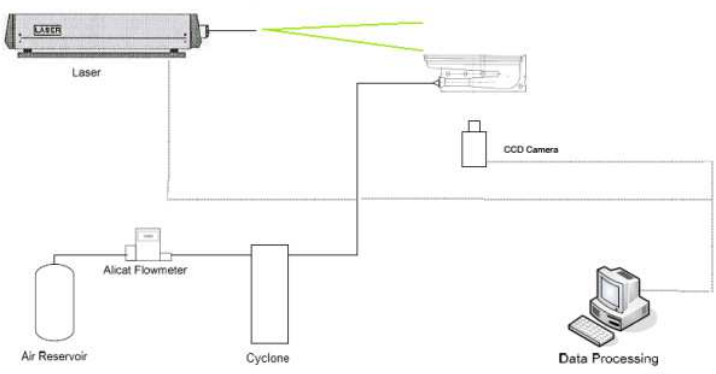

Figure 3 – PIV apparatus schematic diagram.

A light beam is generated by a Dantec Dynamics Nd:YAG laser and is optically transformed into an about 2 mm light sheet plane. Image acquisition is made by a Kodak Megaplus ES1.0 camera, which uses a CCD sensor. Images are processed in an acquisition module which links both the cameras and laser to a computer, where FlowManager 1500 software is used to process data. This module is responsible for the synchronization between the laser pulses and the camera as well as for triggering the laser from the computer.

Once a set of images is acquired, the data corresponding to particles in the first image frame is correlated with the data from particles in the second image frame. It is agreed that it is preferable to divide an image into smaller parts, where in each one a velocity vector is calculated. These regions are commonly called interrogation areas or interrogation windows.

In PIV measurements, several factors must be taken into account. Having in mind the importance of reliable measurements, it is important to choose adequate tracer particles, as well as select adequate time between laser pulses and percentage of interrogation area overlapping. Seeding is made using talcum powder, stored in a cyclone device. In order to confirm if talcum powder is an appropriate seeding agent, a sample is analysed in a CILAS 920 granulometer. Tests lead to a medium diameter of 20 μm for talc powder particles. Knowing that the talc powder density is about 2700 kg/m^3, one can use the following transfer function to estimate the relation between particle velocity and flow velocity:

$$\frac{V_1^*}{V^*} = \frac{\frac{\pi d_p^3}{4}\rho_f \omega j + 3\pi\mu d_p}{\frac{\pi d_p^3}{6}\rho_p + 0.5\rho_f \omega j + 3\pi\mu d_p}$$

It is observed that when talcum powder is immersed in an air flow, particles will respond badly to fluctuations at higher frequencies. Yet, as this work focuses on the average field of velocities (thus, at very low frequencies), it is verified that particles assume the same velocity of the flow and consequently, talcum powder allows appropriate seeding and will be used for PIV measurements along the whole work.

Pressure measurements are carried out to complement PIV results.

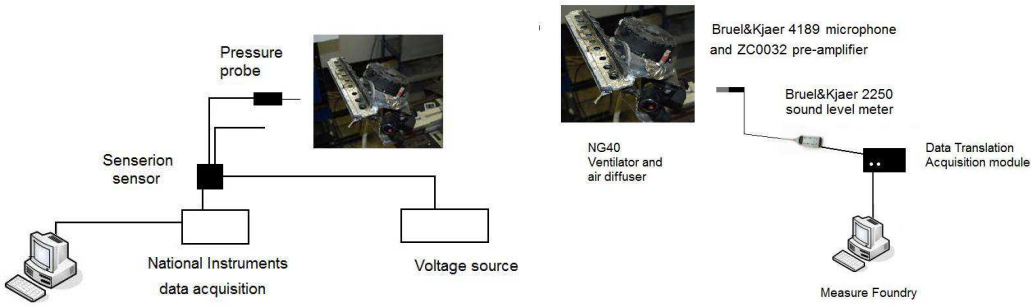

Figure 4 – Apparatus used for static pressure measurements (left) and static pressure fluctuation tests (right).

For static pressure measurements, a pressure probe is connected to a Sensirion SDP1000 thermal differential pressure sensor. The sensor is then linked to a National Instruments DAQ USB6128 acquisition plate. Static pressure fluctuation tests are performed to get more consistent conclusions from pressure tests. This is particularly useful when one needs to verify the existence of recirculation in a flow. The microphone + pre-amplifier set is connected to a Bruel&Kjaer 2250 sound level. The Bruel&Kjaer 4189 microphone features 50 mV/Pa sensitivity and operates in a frequency range from 6.3 Hz to 20 kHz. Bruel&Kjaer sound level is connected to a Data Translation 9841-SB acquisition module, which is responsible to transfer the data to a computer, where it is processed in Measure Foundry software.

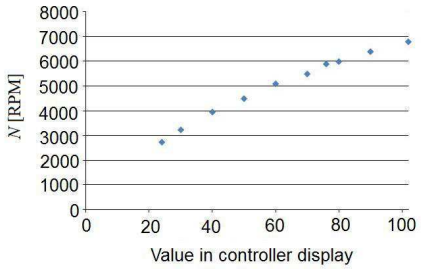

Figure 5 – Rotational speed N vs displayed value in the controller.

The ventilator controller displays a range from 0 to 102, and each value corresponds to a rotational speed. To convert the displayed information to a velocity in rpm, a strobe light is pointed to the ventilator inlet and a single ventilator blade is marked in a contrasting colour. If the flashing frequency of the light is varied, at some moment the signed blade will appear to be *stopped*. When that happens, one can say the rotational speed has the same value of the light flashing frequency, under the precision assured by the strobe. Results for the ventilator's rotational speed *N* are shown in figure 4.

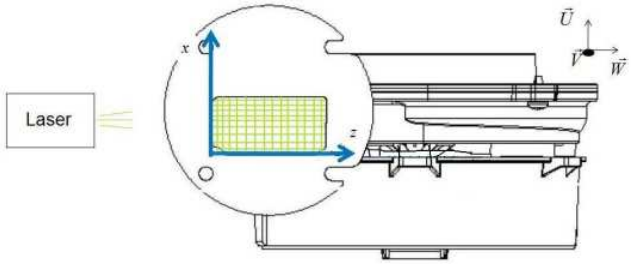

Figure 6 - Top view of the ventilator exit with superposition of the referential used for data processing.

Figure 5 outlines the measured PIV planes and correspondent referential for the tests with the ventilator. U and V are non-dimensionalized by U_{max} and V_{max}. In the same way, x and z are non-dimensionalized by x_{max} and z_{max}. After some tests comparing the results of using various time between pulses, interrogation areas and overlapping percentages, it is decided to select for post-processing the results from 64x64 pixel interrogation areas, as this dimension allows faster calculations than 32x32 pixel and assures a reasonable number of data points. Measured velocities are almost insensitive to the variation of overlapping percentage, for the conditions of this particular flow. Therefore, 50% overlapping is selected, for it represents a good compromise between the larger amount of data computed by 75% overlapping and the smaller processing time guaranteed while using 25% overlapping. In what concerns time between pulses, tests are made using 20 μs, excepting the case of the ventilator test at 5900 rpm, where a 10 μs interval is more adequate.

III -- Test results

Concerning the ventilator characterization, PIV measurements are made for three distinct revolution regimes: N=2740 rpm, N=4500 rpm and N=5900 rpm. From these measurements, vectorial components of velocity are integrated in order to get the volumetric flow rate at the ventilator outlet. The chosen integration method was triangulation with linear interpolation, because it was the simplest method available.

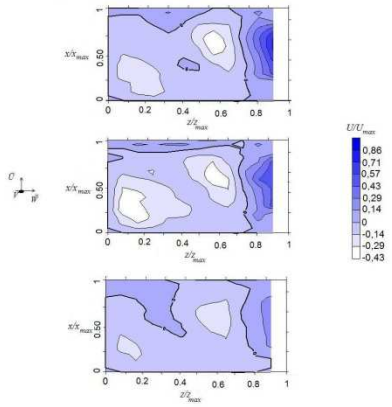

Figure 7 - Iso-region map for U component of velocity. From top to bottom, results for N=5900 rpm, N=4500 rpm *and* N=2740 rpm.

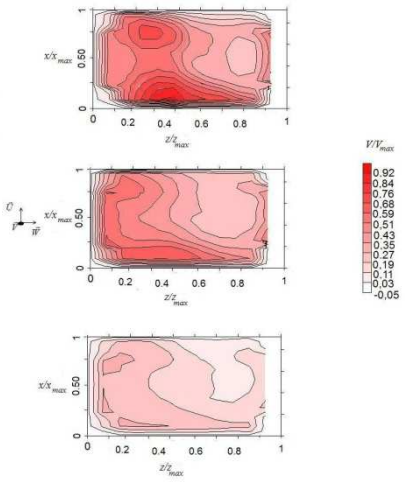

Figure 8 - Iso-region map for V component of velocity. From top to bottom, results for N=5900 rpm, N=4500 rpm *and* N=2740 rpm.

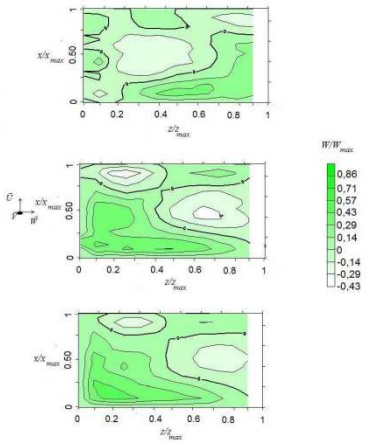

Figure 9 - Iso-region map for W component of velocity. From top to bottom, results for N=5900 rpm, N=4500 rpm *and* N=2740 rpm.

Results are presented in the form of iso-region maps for each tested ventilator rotational speed. Velocity components are represented in a non-dimensional way, dividing each velocity component value for the overall maximum velocity value. Comparing the same velocity component at different rotational speeds, one notices that qualitatively the zones with higher or lower velocity are systematically the same, whatever the rotational speed is. Air flow rate aspirated for the studied rotation regimes is presented in the following table:

N [rpm]	Q [m^3/h]
2740	20.52
4500	47.16
5900	54.00

Table 1 - Aspirated air flow rate for the studied rotation speed.

The ventilator is intended to discharge to a diffuser with circular inlet. Therefore, it is necessary to have a certain length for the flow be distributed in the circular section. Thus, it is important to know the velocity profile at that precise section. To do so, it is made a cardboard circular wall with the same dimension of the inner diameter of the diffuser and is three centimeters high. Results of PIV measurements allow understanding how does the flow evolve from the ventilator exit to the specified section.

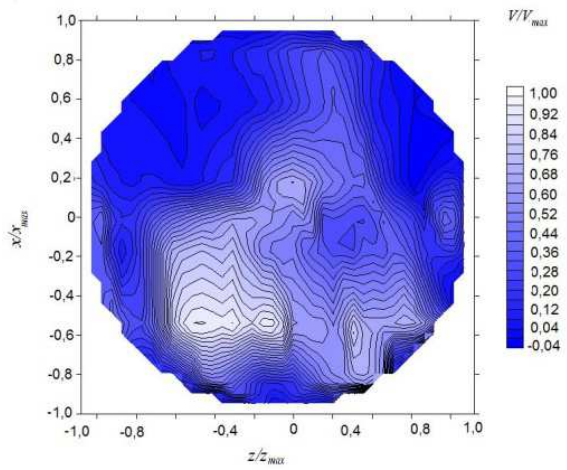

Figure 10 - Spatial distribution of $V=V_{max}$ at 3 mm *downstream the ventilator outlet.*

Figure 10 shows that there are not significant changes in the flow, as the high/low velocity regions rest qualitatively in the same zones.

For the ventilator and diffuser assembly, measurements are made at N=4500 rpm. Two different diffusers are studied: diffuser D1 (comprehends nine interior channels and a plate with circular holes attached at the exit section) and diffuser D2 (is a hollow version of diffuser D1 and has no interior channels, nor plate with holes).

Flow along the exit of diffuser D1 is the first to be characterized. In order to guarantee a good resolution, the assembly is placed so one can divide the diffuser into regions and make measurements for each region separately. The option is to divide the diffuser in three parts, each one with three holes.

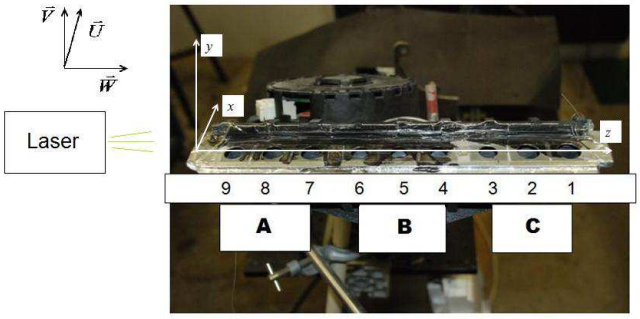

Figure 11 - Numeration attributed to the diffuser holes.

As can be seen in figure 11, the three regions (with three holes each) are named A (for holes 9, 8 and 7), B (for holes 6, 5 and 4) and C (for holes 3, 2 and 1). Velocities at each hole exit are integrated over the respective hole area to obtain the volumetric flow rate passing through the exit holes.

Exit	9	8	7	6	5	4	3	2	1
Q [m^3/h]	2.844	2.592	2.268	1.872	1.116	0.234	1.872	1.440	1.224

Table 2 – Volumetric flow rate for each hole for N=4500 rpm.

Air distribution is not closely uniform. In fact, in the three holes in the centre (6, 5 and 4), there is a substantially lower volumetric flow rate.

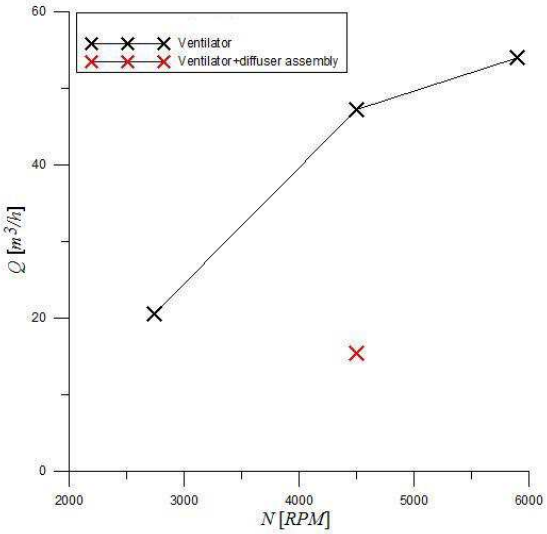

Figure 12 - Q vs N for both ventilator and ventilator and diffuser assembly situations.

The graphic in figure 12 resumes the results from the described PIV measurements. It can be remarked that the attachment of this specific diffuser leads to an air flow that is less than a third of the flow that would be only with the ventilator. This difference can be explained by the head loss induced by the diffuser configuration.

Testing diffuser D2 allows understanding how the flow behaves in the diffuser without the effects of the channels and plate with holes.

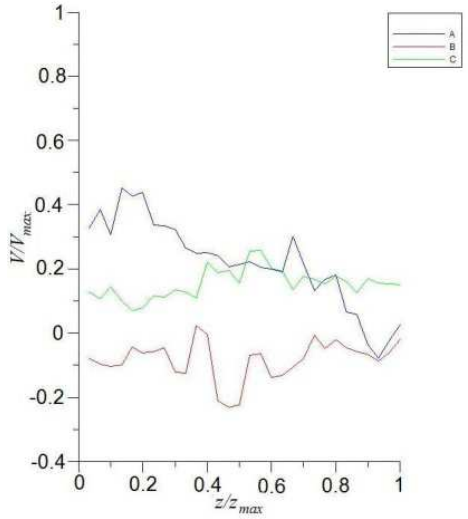

Figure 12 - Spatial distribution of $V=V_{max}$ in diffuser D2 at y=0 mm *and $x=x_{max}$ = 0.22.*

Graphic in figure 12 presents the vertical component of velocity for three regions: A, B and C which correspond to the homonymous regions defined previously. In the presented plane, region B corresponds clearly to a recirculation zone, for $V<0$.

The results obtained from the diffuser D2 reveal that, despite the velocities are in average lower in the diffuser D2 (due to the much bigger exit area of this), when comparing with the results from diffuser D1, one observes that in diffuser D2 velocities in the central zone are higher than in the side zones, which is not the case in the D1 configuration. Therefore, it can be concluded that the plate at the outlet zone does alter the natural tendency of the flow through the diffuser.

Static pressure measurements and fluctuation tests are presented. For what concerns these two kinds of tests, holes were drilled in some points of diffuser D1, as to allow the pressure probe to reach the inner wall of the diffuser.

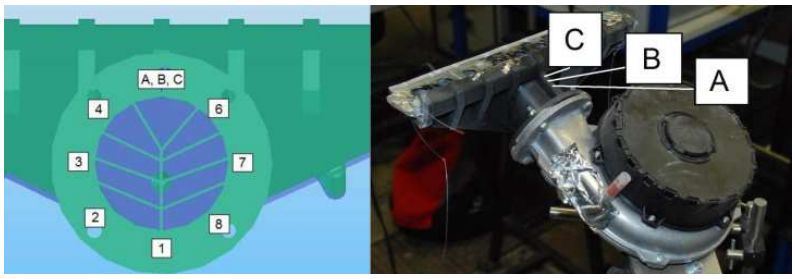

Figure 13 - Schematic view of the numeration attributed to each drilled point.

The numeration attributed to the drilled points is schemed in figure 13.

Pressure take	*N* [rpm]	*p* [Pa] without plate	*p* [Pa] with plate
A	2740	-1.01	4.95
	4500	2.17	22.57
	5900	4.75	41.51
B	2740	-2.40	5.73
	4500	2.54	24.58
	5900	6.78	45.13
C	2740	-0.81	2.89
	4500	2.91	17.25
	5900	7.08	32.88

Table 3 - Average static pressure values for each pressure take.

Table 3 resumes the mean values of static pressure in each point. It shall be noticed that these values are relative to the atmospheric pressure. These results allow to conclude that pressure is always higher when the plate with holes is attached and that for each point, the higher *N* is, the higher *p* will be. Besides, it is important to highlight that attaching the plate makes static pressure in point C be lower than in point B, unlike it happens in the diffuser without plate. This fact suggests that it takes place some perturbation in the flow in the region which drives the air to hole 5.

Static pressure fluctuation tests are a way to assess the evolution of static pressure by the sound generated by the flow inside the diffuser. These tests are run in the same drills than for static pressure measurements. The result is presented in logarithmic scale, the horizontal axis being a frequency (in Hz).

Points 1 to 8 are tested only with diffuser D1 configuration. Peaks at lower frequencies (namely about 45 Hz) are detected in all points but 4 and 6. As those two points correspond respectively to the channels which feed holes 4 and 6 in the diffuser plate, it can be concluded that a recirculation bubble exists in that zone and vortexes are liberated at the measured frequencies. Points A, B and C are tested for either having the plate with holes at the diffuser D1 outlet or not. The reason why special attention is given to these points is their proximity to an abrupt flow change of direction, motivated by the diffuser geometry, which comprehends several angles larger than 15 degrees -- value that White (2008) refers to be the acceptable maximum for a good diffuser performance.

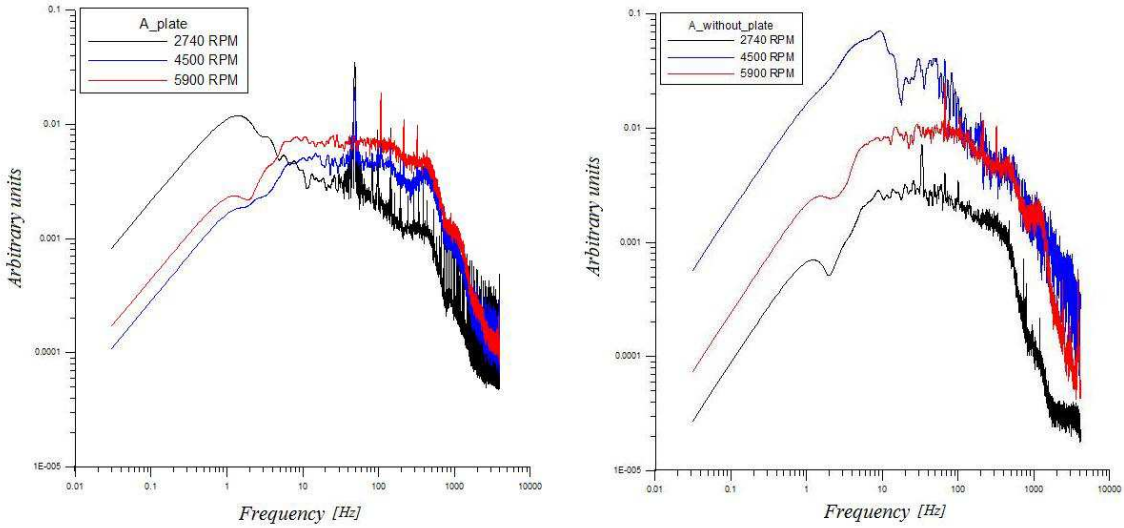

Figure 14 - Spectral analysis of sound for point A in two cases: with attached plate with holes (left) and without plate (right).

Figure 14 shows the spectral analysis for point A for two situations: at the left, the original diffuser D1 configuration and, at the right, the diffuser D1 without plate with holes, allowing to see that, for point A, inserting the plate with holes only *smooths* the peaks at lower frequencies. However, analysing all the other situations, it becomes clear that there are some frequencies in which peaks are preferentially verified, like 45 Hz and the range 90-110 Hz. This cannot be attributed to the system's noise, because despite also presenting peaks at those frequencies, the noise analysis shows clearly that noise is detected at amplitudes typically an order of magnitude below the amplitude of all the sound level measurements.

IV -- **Proposed diffuser configuration**

Since the original diffuser does not assure a homogeneous flow distribution at its outlet, and it has been seen that the plate with holes at the diffuser exit affects significantly the flow, a new configuration for the diffuser channels is proposed. As the velocity profile at the beginning of the diffuser channels is known, it is possible to perform a mass balance between that region and the diffuser outlet. The process occurs in isothermal conditions, so density variations are neglected and the velocity at diffuser outlet is function of initial mean velocity (known from PIV measurements) and geometry. It is presented an estimation of the flow rate distribution in the channels neglecting pressure drops.

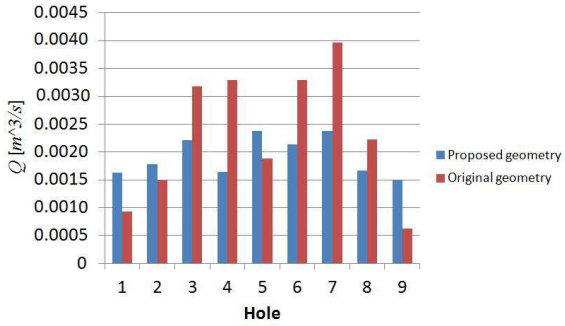

Figure 15 - Flow rate per channel for both the original and proposed channel entrance geometry.

V -- Conclusion

This work had its motivation in a practical problem. The existence of a new water heater technology led to a precise problem: to achieve a homogeneous flow rate distribution for air in the diffuser which feeds the burner system.

PIV measurements proofed velocity is not uniformly distributed along the ventilator exit. In fact, a numerical simulation performed presented in a private report matches clearly the empirical results, as

can be observed in figure 1. The non-uniformity of the flow incoming the diffuser allied to the diffuser's geometry led to a non-homogeneous flow rate distribution at the diffuser outlet. To help understanding the observed flow non-uniformity, static pressure and fluctuation tests were carried out. Both suggest that some perturbation occurs in the flow near the zone which feeds the central holes (4, 5 and 6). Sound level tests permit to conclude that this is a recirculation region, where turbulence is dominant. Possibly, the detected frequency peaks correspond to the vortex spreading frequency. Differences between PIV measurements and the numerical simulation for the case of the ventilator and diffuser assembly can therefore be explained as in some instants there are significantly more particles than in other instants, due to turbulence. As PIV measures the velocity of seeding particles, it means that when it comes an instant when fewer particles are entrained by the flow, the measured velocity will be affected, as in those frames the velocity will be interpreted as zero. This only can be solved by performing measurements during a very long time or by the development of a program that filters frames with concentration of seeding particles below a certain limit.

References

R. J. Adrian. Particle-imaging for experimental fluid mechanics. *Annual Review of Fluid Mechanics*, 23:261-304, 1991.

G. K. Batchelor. *An Introduction to Fluid Dynamics*. Cambridge University Press, 1967.

Bruel & Kjaer. http://www.bksv.com .

P. Coelho and M. Costa. *Combustão*. Edições Orion, 2007.

Dantec. *FlowManager Software and Introduction to PIV Instrumentation -Software User's Guide*.

D. Durox, S. Ducruix, and F. Lacas. Flow seeding with an air nebulizer. Experiments in *Fluids*, 27:408-413, 1999.

Data Translation. http://www.datatranslation.com .

G. N. Duarte. Improvement of the stable limits and primary air entrainment in a single burner of a domestic water heater unit. Master's thesis, Instituto Superior Técnico, 2008.

I. W. Eames, S. Aphornratana, and H. Haider. A theoretical and experimental study of a small-scale steam jet refrigerator. *International Journal of Refrigeration*, 18:378-386, 1995.

E. C. Fernandes, J. G. Merícia, and T. Trindade. Experimental Diagnostics in Thermo-Acoustic Systems. In C. Schram, editor, *VKI Lecture Series*. Von Karman Institute, 2010.

D. P. Hart. The Elimination of Correlation Errors in PIV Processing. *9th International Symposium on Applications of Laser Techniques to Fluid Mechanics*, 1998.

H. R. N. Jones. *The Application of Combustion Principles to Domestic Gas Burner Design*. British Gas, 1989.

N. C. Leitão. Pressure Probe Design. Master's thesis, Instituto Superior Técnico, 2010.

Natalini, SIT Group. http://www.natalini.it .

C. V. Nguyen, A. Fouras, and J. Carberry. Improved accuracy of microPIV measurement using image overlapping technique. *14th Int Symp on Applications of Laser Techniques to Fluid Mechanics*, 2008.

A. K. Prasad. Particle image velocimetry. *Current Science*, 79:51-60, 2000.

R. A. Rato. Experimental Study of Ignition in a Pilot Flame System. Master's thesis, Instituto Superior Técnico, 2009.

F. Rahman, D.B. Umesh, D. Subbarao, and M. Ramasamy. Enhancement of entrainment rates in liquid-gas ejectors. *Chemical Engineering and Processing*, 49:1128-1135, 2010.

M.Raffel, C. E. Willert, S. T. Wereley, and J. Kompenhans. *Particle Image Velocimetry - A practical guide*. Springer, 2007.

D. Satoha, S. Tanakaa, K. Yoshidab, and M. Esashic. Micro-ejector to sup-ply fuel-air mixture to a micro-combustor. *Sensors and Actuators*, 149:528-536, 2005.

L. M. Thomas. Flow Measurements Using Particle Image Velocimetry in the Ultra Compact Combustor. Master's thesis, Air Force Institute of Technology, 2009.

H. C. van de Hulst. *Light scattering by small particles*. John Wiley & Sons, 1957.

J. Westerweel. *Digital Particle Image Velocimetry - Theory and Application*. PhD thesis, Delft University, 1993.

F. M. White. *Fluid Mechanics*. McGraw-Hill, 2008.